International Journal of Physics and Mathematics

E-ISSN: 2664-8644
P-ISSN: 2664-8636
IJPM 2024; 6(1): 05-15

www.physicsjournal.net
Received: 08-11-2023
Accepted: 12-12-2023
Published: 17-01-2024

Nabhan Abdulkareem Hamdon
Department of Petroleum and Refining Engineering, College of Petroleum and Mining Engineering, University of Mosul, Mosul, Iraq

Miyukuzi Takashiki
Department of Physics, Japan National Research Institute Sakai, Osaka, Japan

Corresponding Author:
Nabhan Abdulkareem Hamdon
Department of Petroleum and Refining Engineering, College of Petroleum and Mining Engineering, University of Mosul, Mosul, Iraq

Plasma physics impact on energy and environmental-synthesis and characterization of rGO/$CoSnO_3$ for energy and environmental remediation

Nabhan Abdulkareem Hamdon and Miyukuzi Takashiki

DOI: https://doi.org/10.33545/26648636.2024.v6.i1a.73

Abstract
Graphene oxide was reduced and wrapped around cobalt tin oxide nanoparticles using a simple hydrothermal process. The rGO/$CoSnO_3$ nanocomposite was analyzed using analytical techniques including TG-DTA, XRD, FT-IR, SEM with EDS, XPS, and UV-DRS. TG-DTA analysis verified the melting point and phase transition at a specific calcination temperature. The phase and crystalline size of graphene oxide (GO), reduced graphene oxide (rGO), cobalt oxide (Co_3O_4), cobalt stannate ($CoSnO_3$), and rGO/$CoSnO_3$ are 19.8 nm, 27.6 nm, 26.9 nm, 40.3 nm, and 50.4 nm, respectively. XPS analysis was utilized to investigate the elemental composition and ionic state. The SEM analysis showed that $CoSnO_3$ agglomerated nanoparticles are evenly spread across the surface of rGO, forming a 2D sheet structure. The band gap of rGO, Co_3O_4, $CoSnO_3$, and rGO/$CoSnO_3$ was determined by UV-DRS examination and Kubelka-Munk function diagram analysis, revealing values of 3.5, 2.4, 4.5, 2.7, and 1.6 eV, respectively. We used methylene blue dye for photocatalytic degradation with GO/$CoSnO_3$ nanocomposite and attained a degradation efficiency of 96.2%. The CoSnO3 and rGO/CoSnO3 nanocomposites are utilized as electrode materials in three-electrode and symmetric electrochemical supercapacitors. Electrochemical study shows that $CoSnO_3$ and rGO/$CoSnO_3$ electrodes have high supercapacitance values of 158.8 F/g and 499.7 F/g at a scan rate of 10 mV/s, respectively. The charge-discharge curves of the rGO/$CoSnO_3$ electrode indicated a specific capacitance of 603.12 F/g at 1 A/g, which was higher than the specific capacitance of the $CoSnO_3$ electrode, which was 285.3 F/g at 1 A/g. The rGO/$CoSnO_3$ electrode has a cyclic performance where it maintains 96.2% capacity retention even after 1000 cycles. This research finding could be valuable for mitigating water contamination and utilized as a supercapacitor material.

Keywords: Plasma physics, cobalt oxide, hydrothermal, photocatalytic degradation, methylene blue, cyclic voltammetry

1. Introduction
Environmental contamination has become a significant issue in recent years. Pollutants are steadily rising, leading to significant and irreversible harm to the Earth's environment. Industrial effluents are recognized as the primary cause of water pollution [1-3]. Photocatalytic degradation is a crucial method for treating wastewater by removing toxic heavy organic pollutants. Traditional wastewater treatment procedures have secondary impacts such as high separation costs as well as the production of second-order contaminants through processes including adsorption, coagulation, as well as membrane dissociation, which incur substantial operational expenses. Graphene is considered a viable support material for energy storage batteries due to its ability to enhance charge transfer and mass transport. Graphene oxide also exhibits increased photocatalytic degradation properties. $CoSnO_3$ is a semiconductor compound made of transition metals with a wide-direct band gap. $CoSnO_3$ nanostructures have garnered significant interest for their prospective applications in domains for instance, photocatalytic activity, gas sensors, glucose sensors, and solar cells. Metal oxides typically exhibit superior photocatalytic effectiveness [9, 10]. rGO/ $CoSnO_3$ is the most effective photocatalyst due to its exceptional stability. The development of a novel and efficient nanocomposite is increasingly important since it is an ecologically friendly product. Co_3O_4, $CoSnO_3$, and rGO/ $CoSnO_3$ were utilized to assess Methylene blue dye's deterioration in the presence of sunlight and UV light exposure, and the results were examined and analyzed.

2. Experimental setup

2.1 Materials

The investigation utilized Graphite powder, potassium permanganate, sulfuric acid, and sodium nitrate, Tin chloride ($SnCl_2.2H_2O$), Cobalt chloride ($CoCl_2.6H_2O$), Oxalic acid, and Hydrogen peroxide in their analytical grade without additional purification.

2.2 Synthesis of Graphene Oxide

Graphene Oxide was produced using a modified version of the Hummer's process. 46ml of sulfuric acid, 1g of graphite powder, and sodium nitrate were combined in a beaker and stirred at 500 rpm for one hour. 6 grams of KMnO4 was added gradually to the solution and left to stir for 30 minutes in an ice bath at 37 °C. Additionally, 50ml of water was added slowly, and the mixture was cooled to ambient temperature before being heated to 100 °C. Subsequently, 10ml of H_2O_2 was added to facilitate the synthesis of graphene oxide [15].

2.3 Synthesis of Reduced Graphene Oxide

400 mg of powdered graphene oxide (0.1 mg/mL) was dissolved in 20 ml of water. Then, 10 ml of hydrogen hydrate was added as a reducing agent to decrease the graphene oxide. The mixture underwent centrifugation at a speed of 4000 revolutions per second for 40 minutes following 30 minutes of stirring on a magnetic stirrer at a temperature of 60 °C. The mixture was rinsed with ethanol and distilled water, then dried at 120 °C for 24 hours.

2.4 Synthesis of Cobalt Oxide

Cobalt oxide is frequently produced by the hydrothermal technique in a standard synthesis process. 1.6 grams of cobalt chloride hexahydrate and 0.6 grams of oxalic acid were dissolved in 70 milliliters of water. The mixture was continuously whirled for 30 minutes at room temperature. The mixture was placed in a Teflon-lined stainless steel autoclave and maintained at a temperature of 120 °C for a duration of 12 hours. The product was washed with water and ethanol to remove impurities then dehydrated at 80 °C using air cooling. The material was annealed at 400 °C for 5 hours in a muffle furnace [18].

2.5 Synthesis of Cobalt Tin Oxide

1.6 grams of cobalt chloride dihydrate and 0.6 grams of oxalic acid were dissolved in water. 0.9 grams of tin(II) chloride dihydrate was added gradually. The solution was agitated incessantly for 30 minutes at room temperature. The blend was placed in a Teflon-coated stainless steel autoclave and maintained at 120 °C for 12 hours. The product was washed with water and ethanol to remove any remaining ions, then dried at 80 °C in the atmosphere. The powder underwent annealing at 450 °C for 5 hours in a muffle furnace [19].

2.6 Synthesis of rGO/$CoSnO_3$ Nanocomposite

30 mg of reduced graphene oxide (rGO) was sonicated for 10 minutes with the gradual addition of 1.6 g of $CoCl_2.2H_2O$, 0.9 g of $SnCl_2.2H_2O$, and 0.6 g of oxalic acid. The solution was agitated consistently for 30 minutes at ambient temperature. The mixture was placed in a Teflon-lined stainless steel autoclave and kept at 120 °C for 12 hours. The final product was cleaned with ethanol and water, dried at 80 °C, and then heated at 450 °C for 5 hours in a muffle furnace.

3. Results and Discussion

3.1 Thermal Gravimetric - Differential Thermal Analysis (TG-DTA)

The thermal stability of produced Co_3O_4 and $CoSnO_3$ nanoparticles was examined by TG-DTA analysis. The nanomaterials were heated from room temperature to 1100 °C at a rate of 20 °C per minute in an air environment. DTA techniques were used to study the thermal properties of produced $Co(OH)_2$ nanoparticles. $Co(OH)_2$ experienced thermal decomposition in three stages. The initial weight loss from room temperature to 130 °C was caused by the removal of free water through dehydration and evaporation, leading to a 14% decrease in weight [22]. A second weight loss occurs between 130 °C and 230 °C, with around 15% of unnecessary moisture being lost. The third weight loss occurs at approximately 28% between 230 °C and 700 °C. At temperatures exceeding 700 °C, Co_3O_4 is formed and remains stable without any loss of mass, demonstrating the thermal stability of the crystalline Co_3O_4 sample. The exothermic peak about 700 °C was clearly observed due to the decalescence phenomenon, likely caused by the transition from the amorphous to the crystalline phase. Figure 1 shows the TG-DTA curve of $CoSn(OH)_2$ [23]. The initial weight loss occurs at 160 °C, representing approximately 22% of the total weight loss, which is attributed to dehydration and the elimination of free water from the initial precursor. At 850 °C, an extra 43% weight loss occurs as a result of the dehydration of CoSn(OH)2. The calcination temperature of $CoSn(OH)_2$ is determined to be 500 °C based on TG-DTA analysis [26-27]. The TGA study has verified the necessary temperature range for the $CoSnO_3$ nanocomposite that was synthesized.

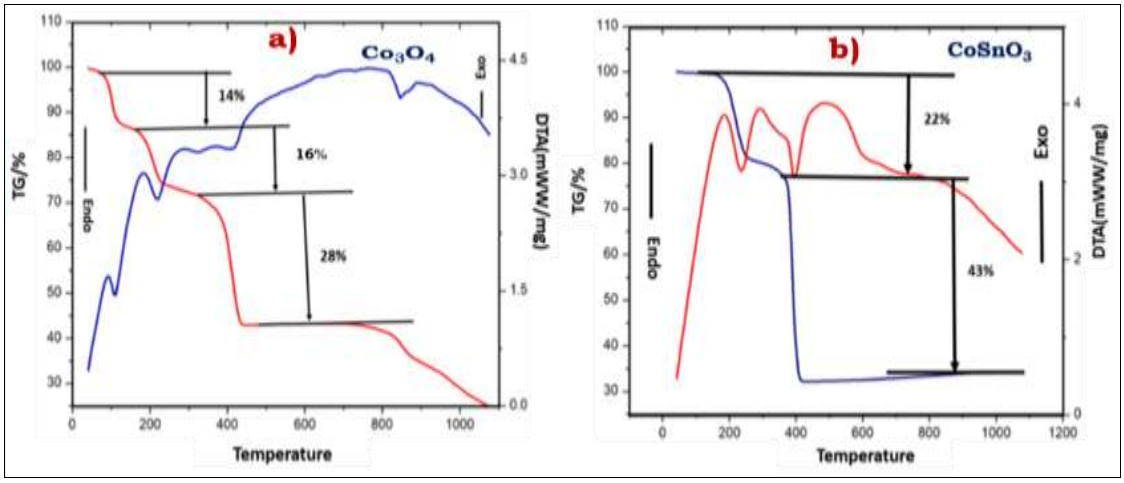

Fig 1: TG-DTA Analysis of (a) $CoSnO_3$ and (b) rGO/$CoSnO_3$ nanocomposites

3.2 XRD Analysis

The TG-DTA analysis showed the presence of $CoSnO_3$ and rGO/ $CoSnO_3$ nanocomposite. The X-ray diffraction (XRD) patterns of the samples, post-calcination at 500 °C, revealed diffraction peaks at 2θ values corresponding to the planes (220), (422), and (511) of Co_3O_4 nanoparticles, as per JCPDS Card No. 42-1467 [28]. The $CoSnO_3$ composite exhibits reflections on the planes (211), (220), (400), (422), and (511), which correspond well with JCPDS Card No. 29-0514 [29-30]. The $CoSnO_3$ nanoparticle production started at around 450 °C during calcination [30]. No peaks are observed in other phases, demonstrating the excellent purity of the compounds depicted in (Fig.2). The various characteristics, including the crystallite size of the rGO/ $CoSnO_3$ nanocomposite, are determined using the Debye–Scherrer formula (Equation 1) and are listed in Table 1 [31].

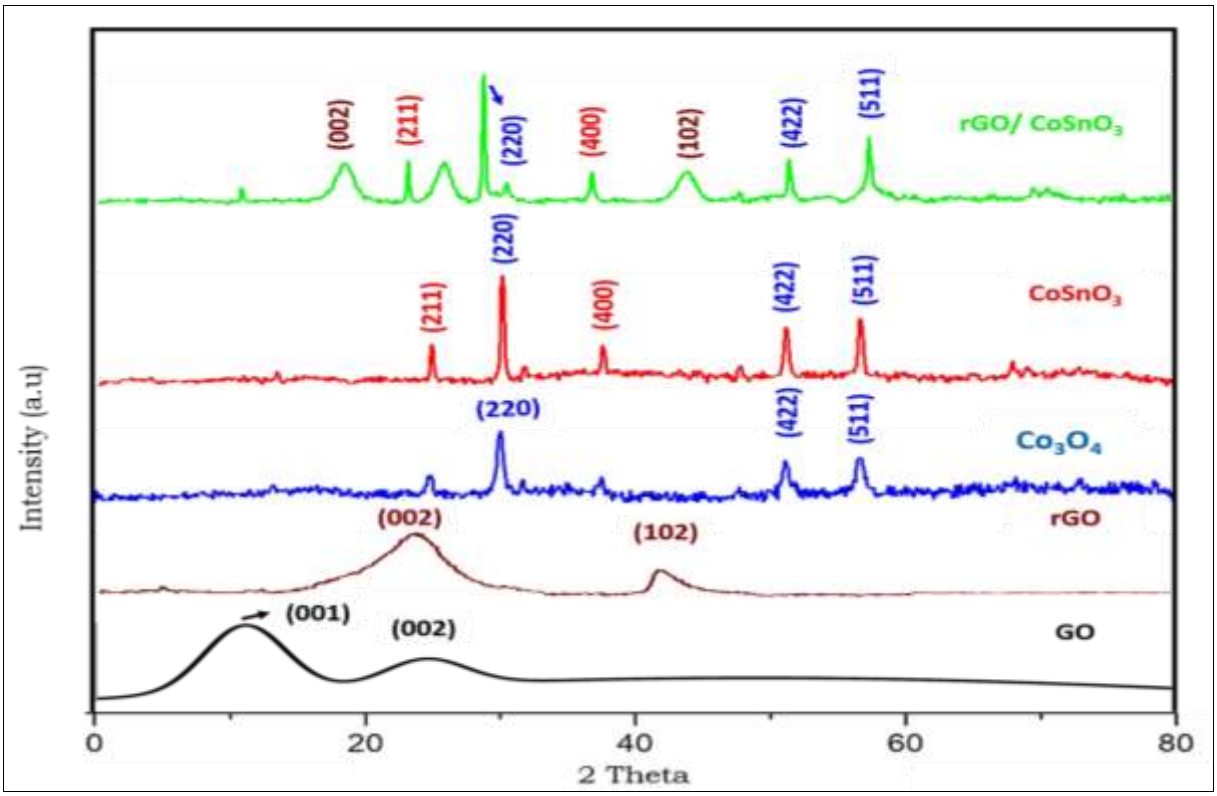

Fig 2: XRD spectra of (a) GO, (b) rGO, (c) Co_3O_4, (d) $CoSnO_3$ and (e) rGO/$CoSnO_3$

3.2.1 Debye–Scherer's equation

$$\text{Crystalline size (D)} = \frac{0.9\lambda}{\beta \cos\theta} \quad (1)$$

Where λ is the wavelength (λ = 1.5406 Å (Cu Kα), β is the full width half maximum (FWHM) and θ is the diffraction angle.

Table 1: Crystalline size of Co_3O_4, $CoSnO_3$ and rGO/$CoSnO_3$ nanocomposite

S. No	Sample	Crystaline Size(nm)
1.	GO	19.8
2.	rGO	27.6
3.	Co_3O_4	26.9
4.	$CoSnO_3$	40.3
5.	rGO/$CoSnO_3$	50.4

3.3 FT-IR Spectrum of rGO/$CoSnO_3$ Nanocomposite

FT-IR is a powerful method for analyzing the many functional groups present in graphene oxide, particularly those related to oxygen. The FT-IR spectra of GO in Fig.3 confirmed the successful oxidation of the graphite. Figure 3b displays absorption stretching vibration peaks at 1099 cm^{-1} and 1623 cm^{-1}, corresponding to the stretching of C-O and C=O groups. Additionally, the vibration band at 1392 cm^{-1} is attributed to the stretching mode of the H-O-H group in rGO. The peaks at 566 cm^{-1} and 665 cm^{-1} correspond to the stretching vibrations of the Co-O bond in Figure 3c. The pure $CoSnO_3$ exhibited distinctive bands, notably the H-O-H bond at 3419 cm^{-1} as shown in Fig.3d, which align well with previously published values. The band at 540 cm^{-1} in the rGO/ $CoSnO_3$ composite is attributed to the metal-oxygen stretching vibration. This co-existence is important as it hinders the recombination of charge carriers and boosts the supercapacitor and catalytic properties of the nanocomposite through a synergistic effect.

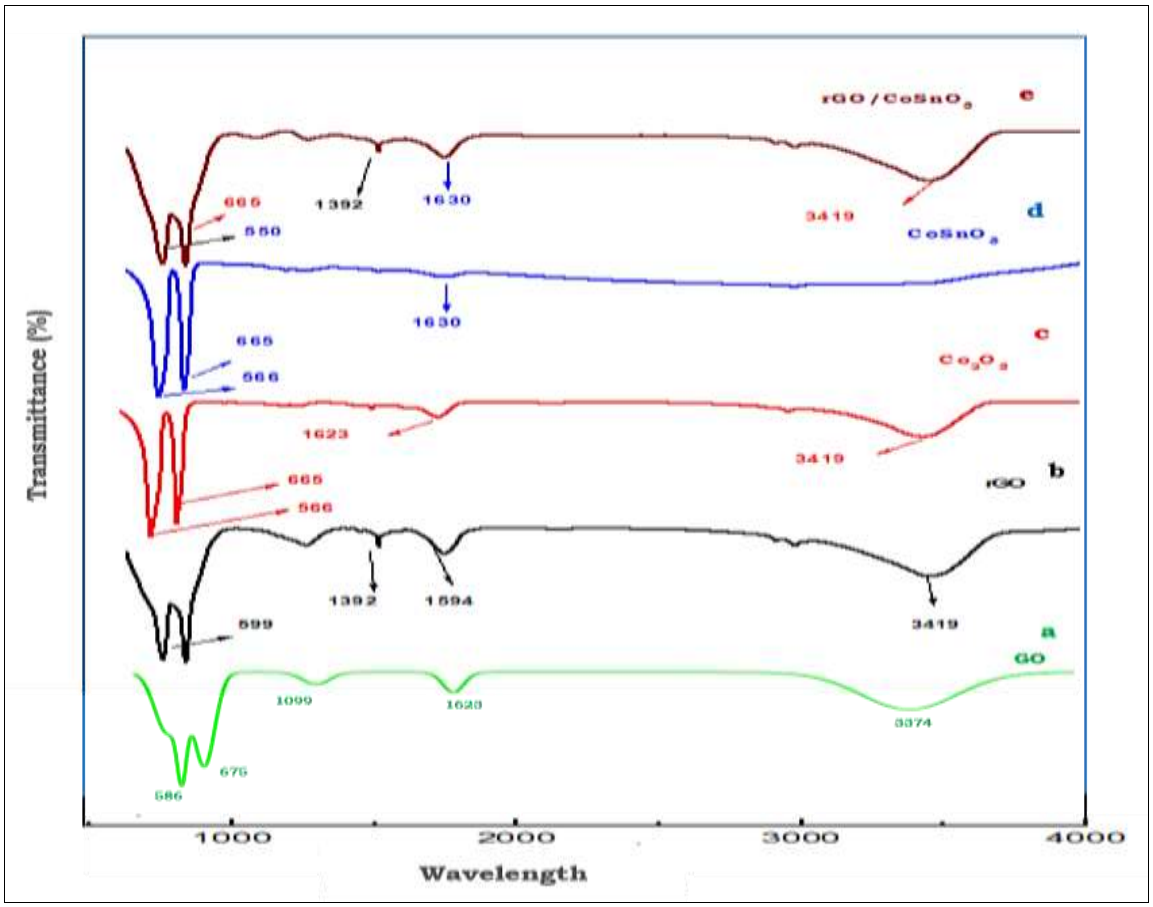

Fig 3: FT-IR Spectrum of (a) GO, (b) rGO, (c) Co_3O_4, (d) $CoSnO_3$ and (e) rGO/$CoSnO_3$

3.4 XPS analysis

The elemental composition and chemical state of prepared nanocomposite confirmed by X-Ray Photoelectron Spectroscopy. The XPS spectra Fig.4a shows that the existence of Sn, Co, O and C elements in composite. Fig.4b show the C1s and the Co_3O_4 binding energy observed at 781.7eV crrosponding to $Co2p^{1/2}$ respectivly (Fig.4c). Fig.4d display the high resolution spectrum of Sn 3d where binding energy at 495.3 and 486.7 eV charateristic of $3d^{3/2}$ and $3d^{5/2}$, respectively which is in agrement with Sn^{2+} state. The XPS spectra of Co 2p shows in fig.2b, Co 2p binding energy procured at 781.7 eV and O1s having 532 eV binding energy (Fig.4e). With the aforementioned results would suggest that purity of the synthesized nanocomposite.

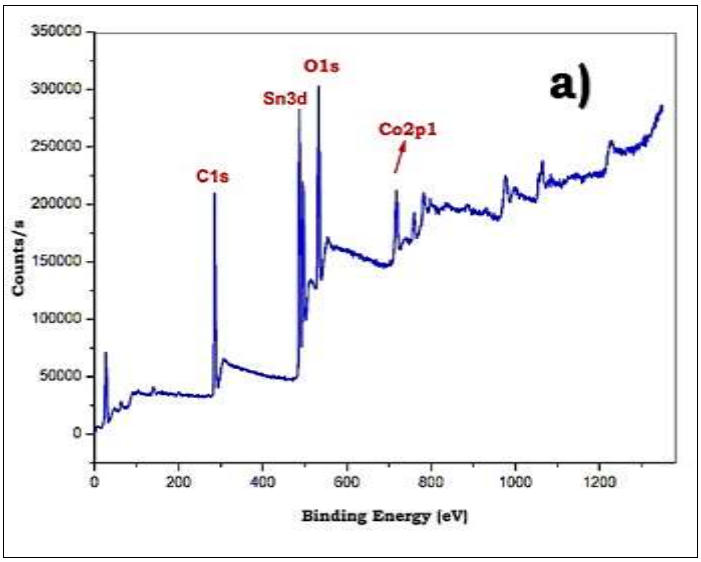

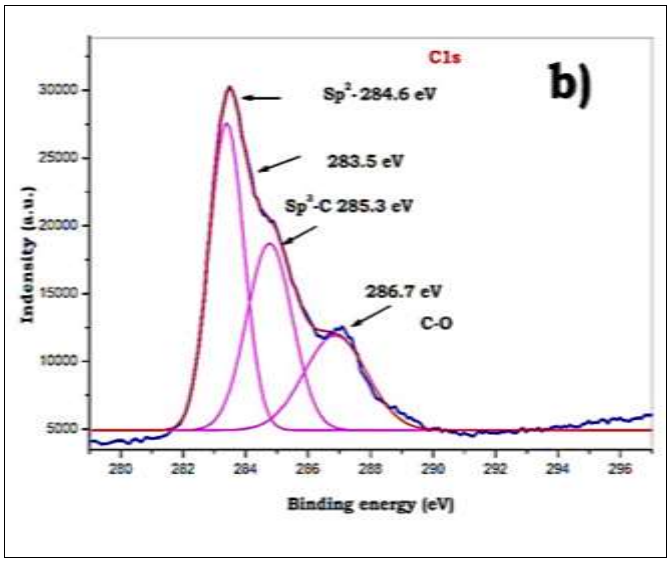

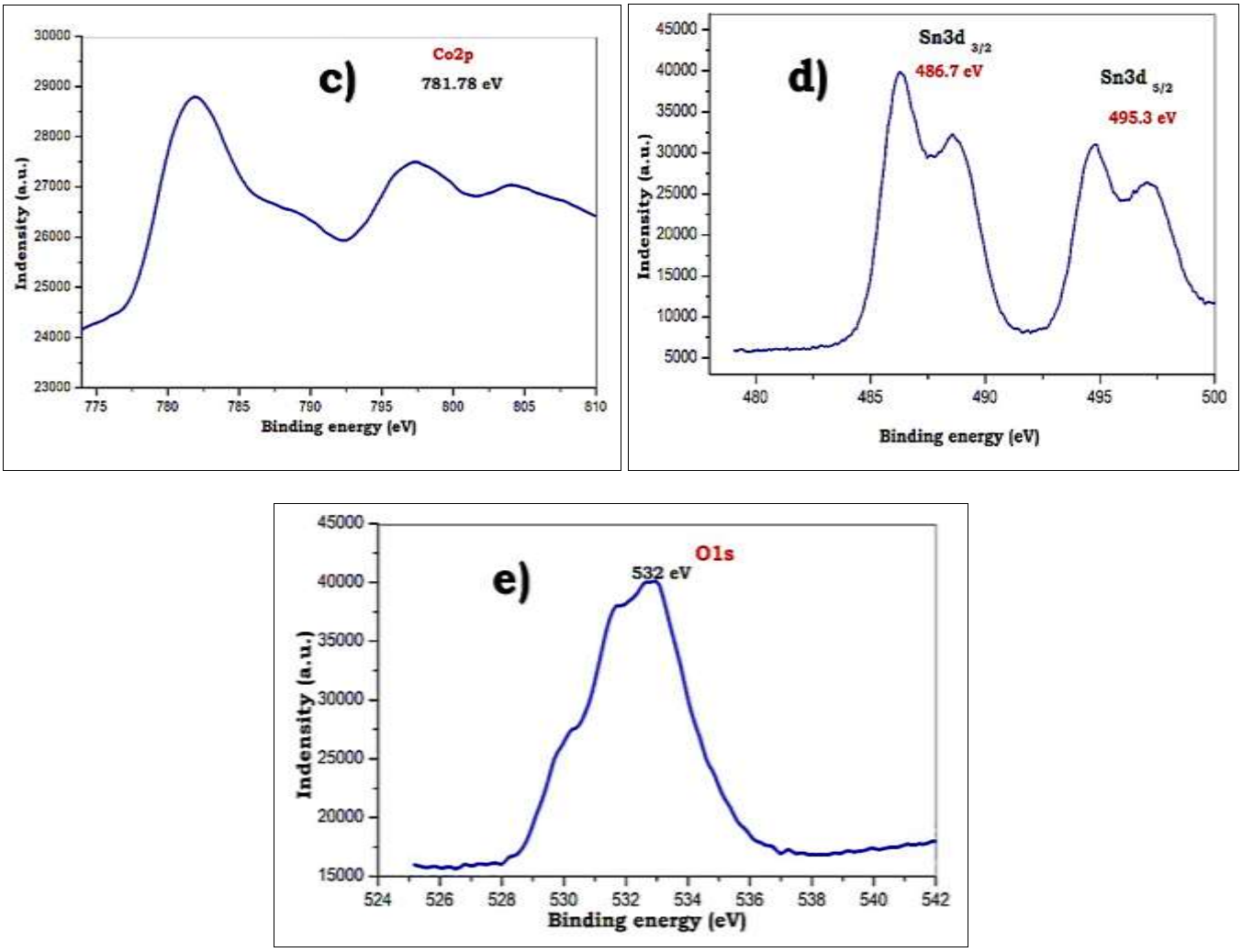

Fig 4: XPS Spectra of rGO/$CoSnO_3$ a) survey spectrum, b) C1s spectrum, c) Co2p spectrum, d)Sn3d spectrum and e) O1s spectrum

3.5 Correlation of Photocatalytic Activity with Band Structure

Using a catalyst and an irradiation source, photocatalysis accelerates a photoreaction. Free radicals like hydroxyl radicals (•OH) are the driving force behind photocatalysis processes, and the capacity of the catalyst to produce electron–hole pairs is critical. As the photocatalyst's optical sensitivity shifts to longer excitation wavelengths, its band gap energy decreases. Photocatalyst band gaps may be reduced using a variety of techniques. Band gap is inversely proportional to catalytic activity (equ-4). The rGO/$CoSnO_3$ has the lowest band gap energy value (1.6 eV) compared to bare materials (Co_3O_4 = 4.5eV, $CoSnO_3$ = 2.7eV) hence the material exhibited a high Photocatalytic property.

$$\text{Band gab} \propto \frac{1}{\text{Catalytic Property}} \quad (4)$$

S. No	Sample	Band gap (eV)	Degradation percentage (%)	
			Sunlight	UV-Light
1.	Co_3O_4	4.5	83.6%	62.0%
2.	$CoSnO_3$	2.7	85.8%	72.0%
3.	rGO/$CoSnO_3$	1.6	96.2%	75.2%

3.6 Correlation of Photocatalytic Activity with crystallite size

For this work, micrometer-sized particles were used to reduce the influence of other catalytic characteristics (such as excessive surface area and quantum confinement effect) on photocatalytic experiments.

In continuous process conditions, the findings showed that the photocatalytic capabilities were highly reliant on the crystallinity of the material. Increases in crystallite size have a significant impact on the accelerated photodecomposition of organic matter. The propensity for crystallite size to have an effect was further demonstrated by altering the quantity of catalysts in the photocatalytic reaction. The rGO/$CoSnO_3$ nanocomposite having a larger particle size (50.4nm**)** compared to bare materials (Co_3O_4 = 26.9 and $CoSnO_3$ = 40.3) inferred that the nanocomposite of rGO/$CoSnO_3$ was easily degrading the dye molecules.

$$\text{Crystalline size} \propto \text{Catalytic Property} \quad (5)$$

S. No	Sample	Crystalline Size (nm)	Degradation percentage (%)	
			Sunlight	UV-Light
1.	Co_3O_4	26.9	83.6%	62.0%
2.	$CoSnO_3$	40.3	85.8%	72.0%
3.	rGO/$CoSnO_3$	50.4	96.2%	75.2%

3.7 Morphology Analysis

SEM micrographs were used to study the surface morphology of the prepared rGO, Co_3O_4, $CoSnO_3$, and rGO/ $CoSnO_3$. The SEM pictures in Fig.5.a-e reveal that GO and rGO had a sheet-like structure. The $CoSnO_3$ nanoparticle appeared in an agglomerated form. Figure 5c displays the cubic surface

morphology of Co_3O_4. The rGO/ $CoSnO_3$ nanocomposite exhibited $CoSnO_3$ nanoparticles in a cubic form scattered across the rGO surface in various orientations.

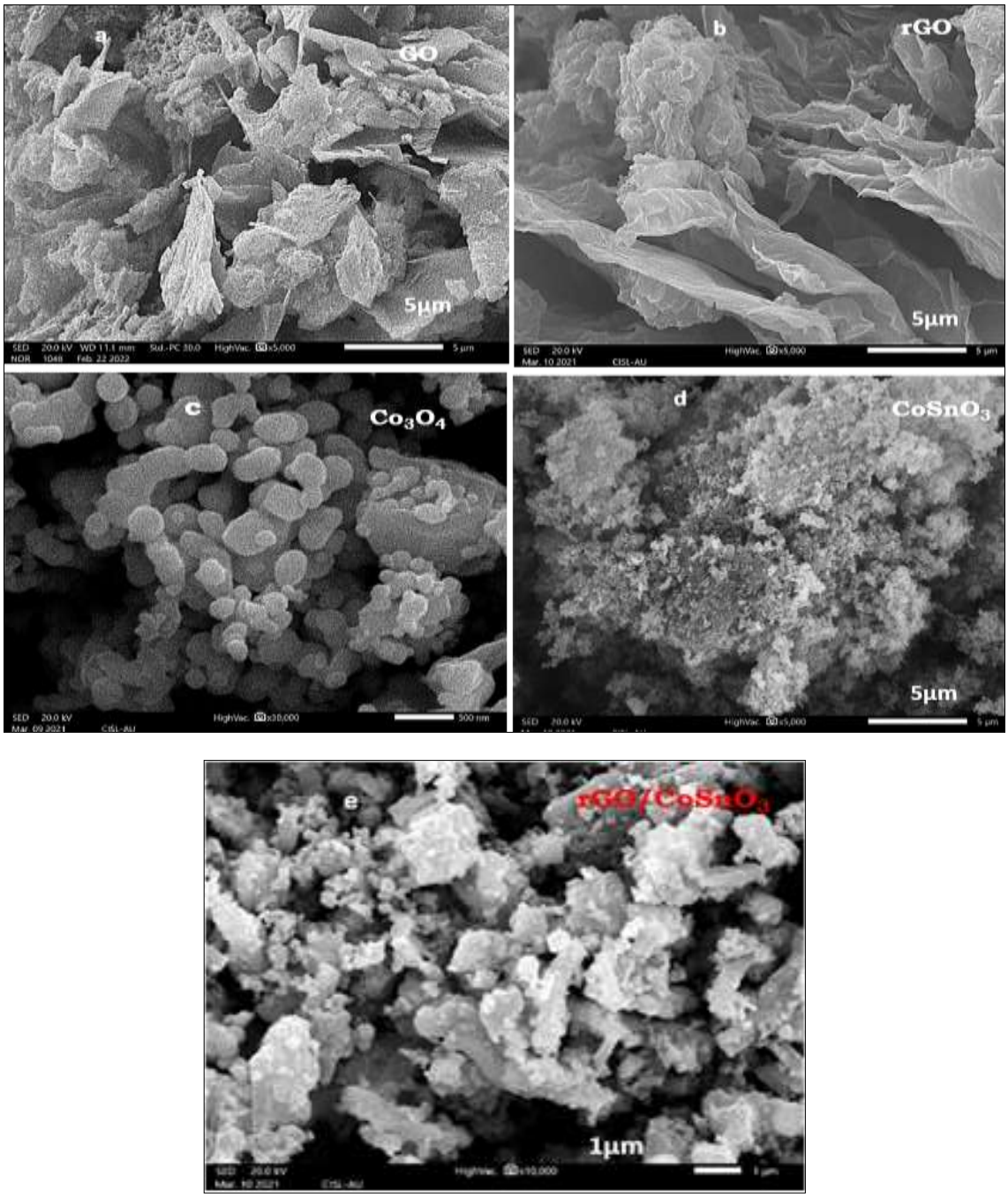

Fig 5: SEM analysis of GO, rGO, Co_3O_4, $CoSnO_3$ and rGO/$CoSnO_3$

3.8 EDX Analysis of rGO, Co_3O_4, $CoSnO_3$ and rGO/$CoSnO_3$ nanocomposite

The EDX analysis was used to interpret the elemental and chemical composition of the prepared nanocomposite. The EDX spectrum of rGO, Co_3O_4, $CoSnO_3$, rGO/$CoSnO_3$ nanocomposite revealed a homogeneous distribution of C, O, Co and Sn in the rGO/$CoSnO_3$ composite. The percentage of C, O, Co and Sn in the nano material was carried out according to the EDX analysis (Fig.6). The quantitative analysis of EDX revealed that the atomic ratio of Co: Sn was 1:3.

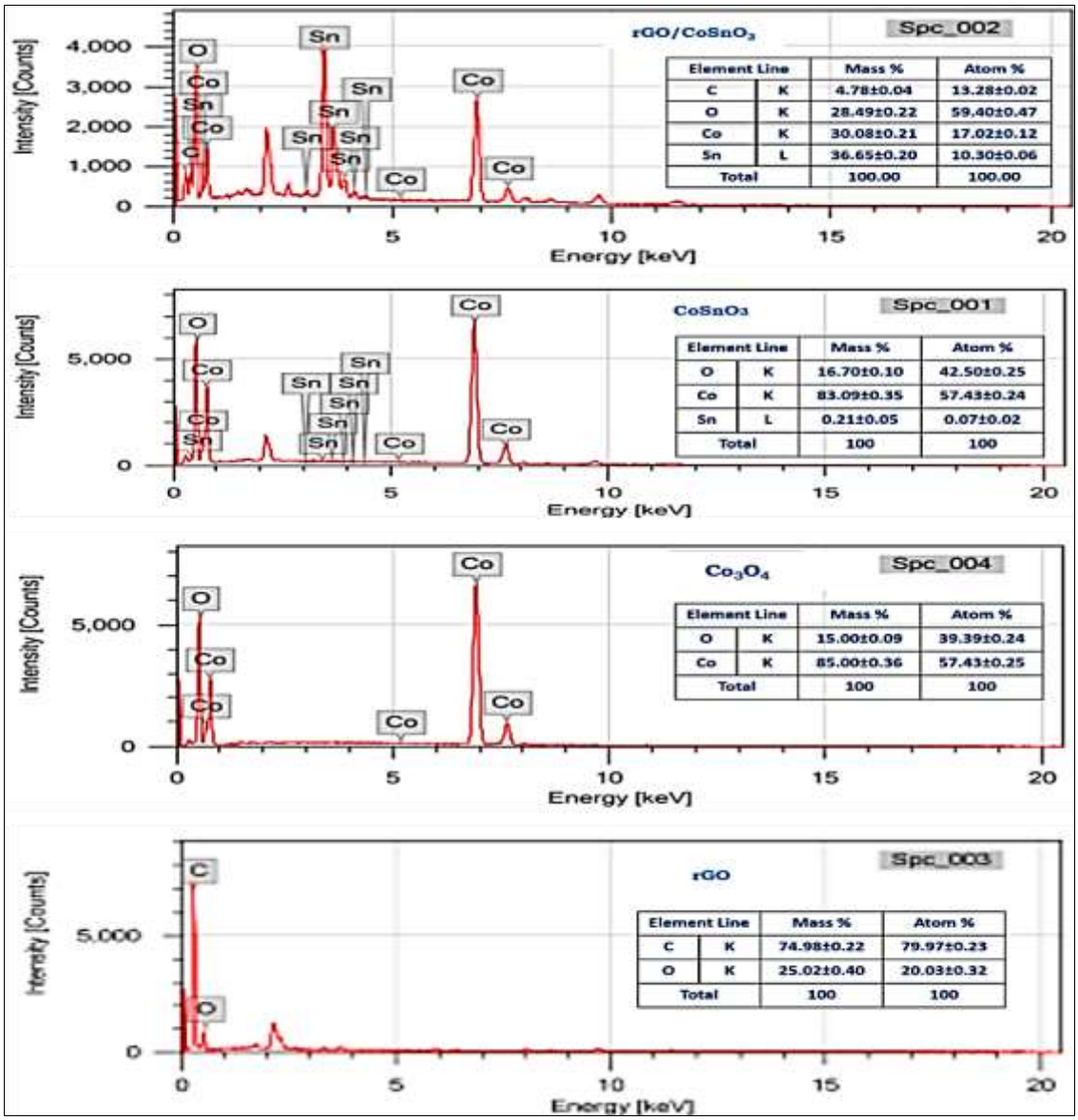

Fig 6: EDS analysis of rGO, Co_3O_4, $CoSnO_3$and rGO/$CoSnO_3$

3.9 UV - DRS Analysis

UV diffuse reflectance spectroscopy was conducted on graphene oxide (GO), reduced graphene oxide (rGO), Co_3O_4, $CoSnO_3$, and rGO/ $CoSnO_3$ nanocomposite. The results in Fig.7 indicate that pure Co_3O_4 nanoparticles displayed a notable UV absorption edge at 800 nm. However, the UV absorption of other samples changed towards longer wavelengths. The variations in the absorption edges indicate alterations in the band structure. The bandgap of samples is obtained using the Kubelka-Munk function equation.

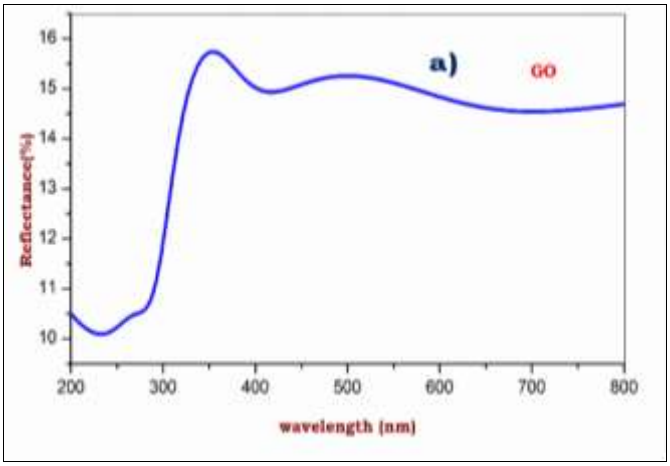

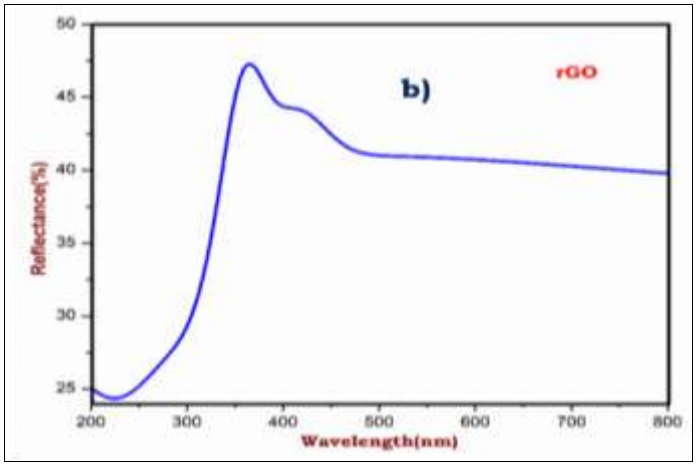

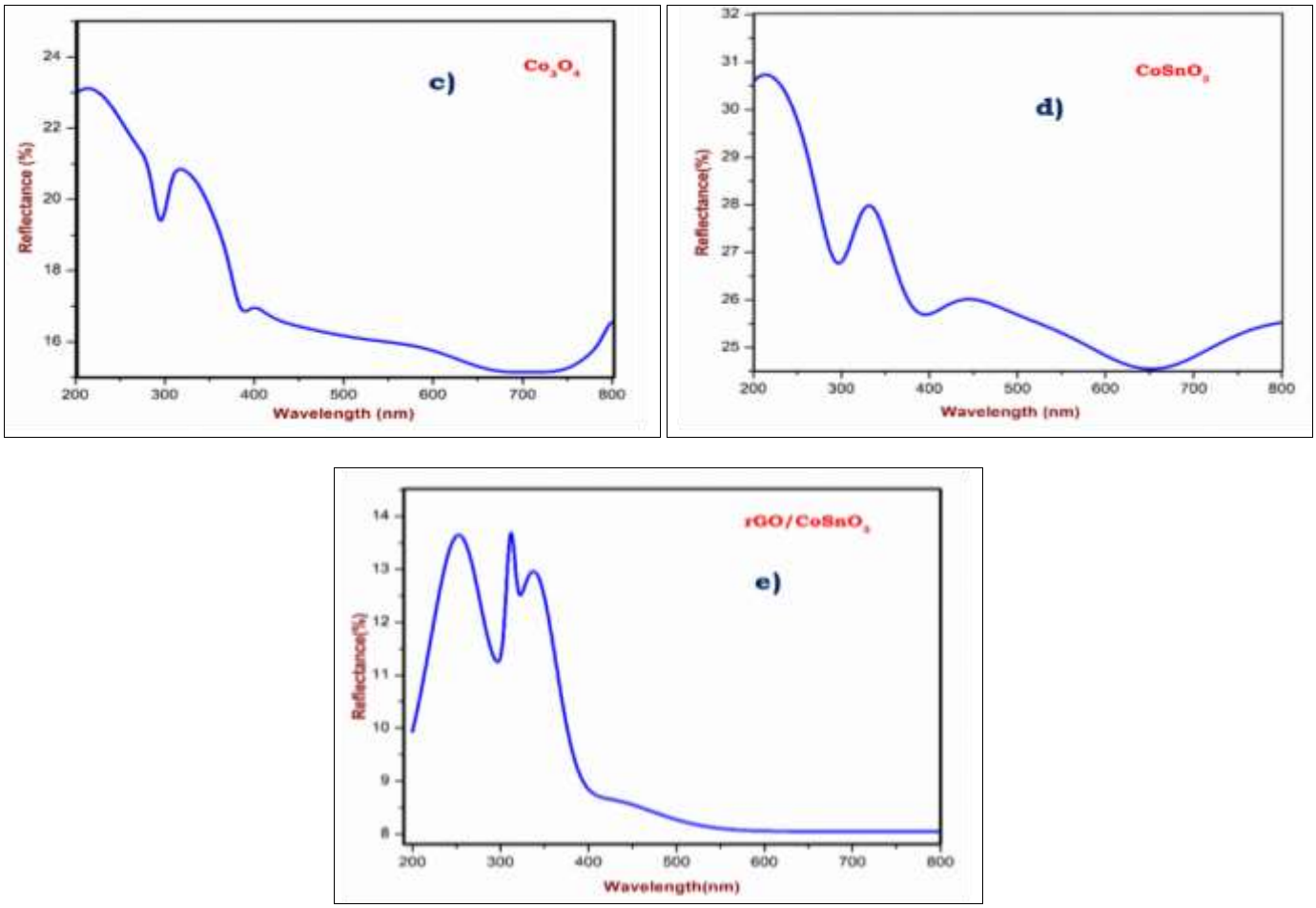

Fig 7: UV-DRS Image of (a) GO, (b) rGO, (c) Co_3O_4, (d) $CoSnO_3$ and (e) rGO/$CoSnO_3$

$$\alpha h\nu = A\,(h\nu - E_g)n \quad (2)$$

α represents the absorption coefficient and hν stands for the incident photon energy. The bandgap energies are derived from the intercept of the tangents, as illustrated in Figure 8. The band gaps of the produced materials are as follows: GO (3.5 eV), rGO (2.4 eV), Co_3O_4 (4.5 eV), $CoSnO_3$ (2.7 eV), and rGO/ $CoSnO_3$ nanocomposite (1.6 eV). Oxygen vacancies can provide impurity levels close to the valence band, resulting in a reduced band gap value and higher catalytic activity in rGO/ $CoSnO_3$ compared to GO, rGO, Co_3O_4, and $CoSnO_3$ materials.

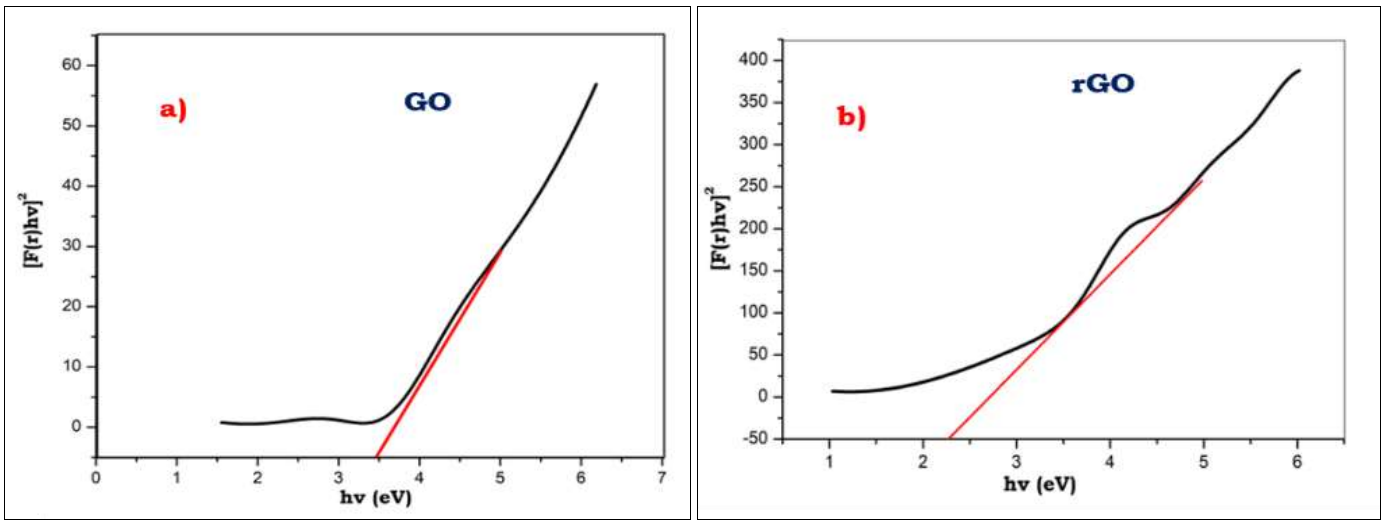

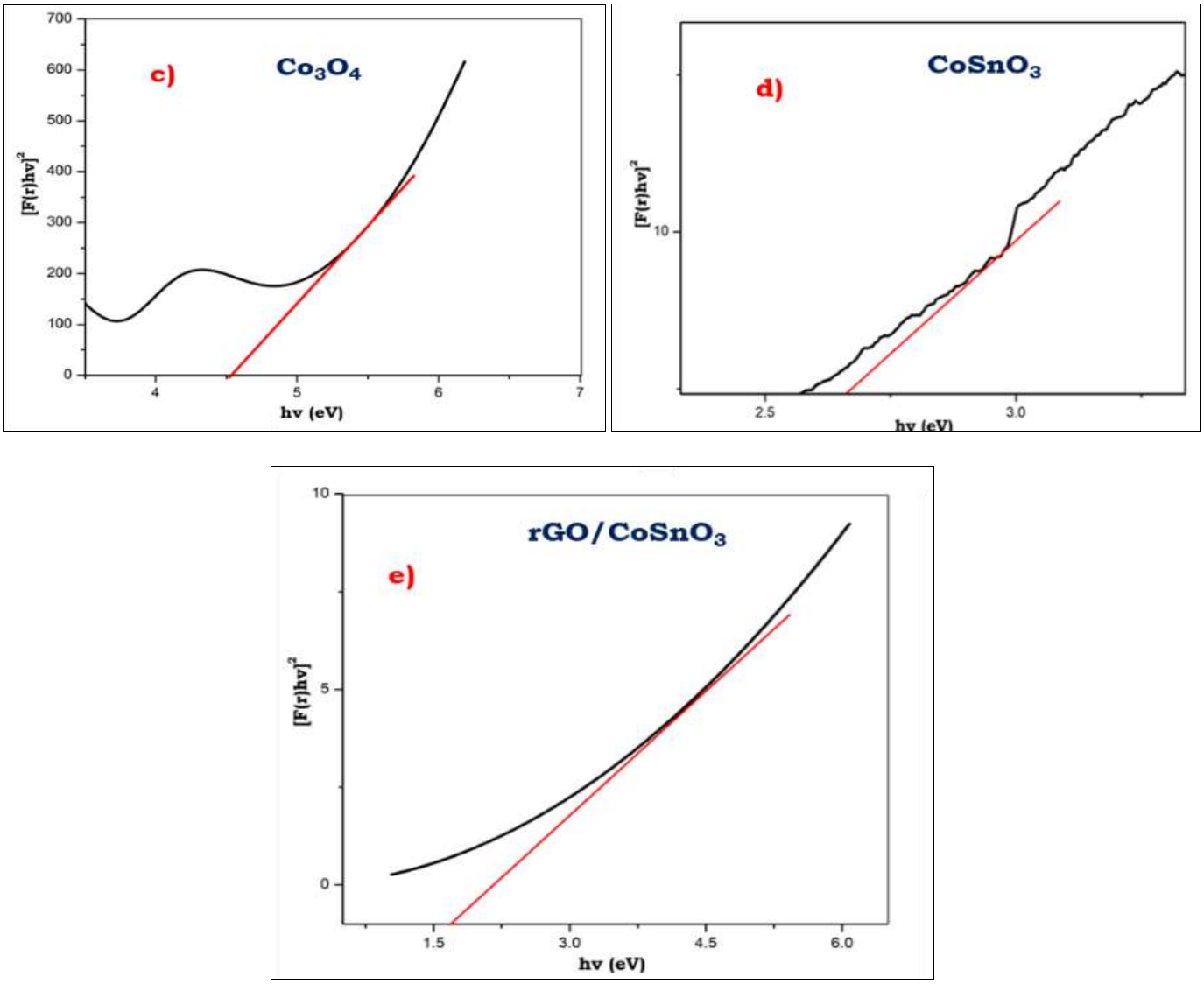

Fig 8: Tauc's Plot of (a) GO, (b) rGO, (c) Co_3O_4, (d) $CoSnO_3$ and (e) rGO/$CoSnO_3$

Degradation percentages gradually increased with increasing the weight percentage of the catalyst and compared to the irradiation of sunlight and UV-light, sunlight irradiation is most preferred and efficient process for the photocatalytic degradation process.

Table 2: Comparison of Degradation Percentage under Sun-light Irradiation

S. No	Weight of Catalyst	Sample	Dye	Irradiation	Percentage (%)
1	10mg	Co_3O_4	Methylene blue	Sunlight	75.2%
	10mg	$CoSnO_3$	Methylene blue	Sunlight	85.3%
	10mg	rGO/$CoSnO_3$	Methylene blue	Sunlight	88.2%
2	20mg	Co_3O_4	Methylene blue	Sunlight	77.2%
	20mg	$CoSnO_3$	Methylene blue	Sunlight	88.3%
	20mg	rGO/$CoSnO_3$	Methylene blue	Sunlight	92.0%
3	30mg	Co_3O_4	Methylene blue	Sunlight	83.6%
	30mg	$CoSnO_3$	Methylene blue	Sunlight	85.8%
	30mg	rGO/$CoSnO_3$	Methylene blue	Sunlight	96.2%

Table 3: Comparison of Degradation Percentage under UV-light Irradiation

S. No	Weight of Catalyst	Sample	Dye	Irradiation	Percentage (%)
1	10mg	Co_3O_4	Methylene blue	UV-light	40.0%
	10mg	$CoSnO_3$	Methylene blue	UV-light	44.4%
	10mg	rGO/$CoSnO_3$	Methylene blue	UV-light	48.0%
2	20mg	Co_3O_4	Methylene blue	UV-light	55.3%
	20mg	$CoSnO_3$	Methylene blue	UV-light	57.0%
	20mg	rGO/$CoSnO_3$	Methylene blue	UV-light	72.0%
3	30mg	Co_3O_4	Methylene blue	UV-light	62.0%
	30mg	$CoSnO_3$	Methylene blue	UV-light	72.0%
	30mg	rGO/$CoSnO_3$	Methylene blue	UV-light	**75.2%**

4. Conclusion

Nanomaterials such as GO, rGO, Co_3O_4, $CoSnO_3$, and rGO/ $CoSnO_3$ were synthesized using the hydrothermal method. After calcination at 450 °C for 6 hours, cobalt oxide and cobalt tin oxide transformed into Co_3O_4 and $CoSnO_3$, resulting in the formation of rGO/ $CoSnO_3$ nanomaterials. The nanomaterials exhibited crystalline sizes of 26.9 nm, 40.3nm, and 50.4 nm, and possessed cubic and agglomerated structures. The Kubelka-Munk function plot analyzed the band gaps of rGO, Co_3O_4, $CoSnO_3$, and rGO/ $CoSnO_3$ as 3.0, 3.5, 2.4, 4.5, 2.7, and 1.6 eV, respectively. The photocatalytic efficiency of the prepared Co_3O_4, $CoSnO_3$, and rGO/ $CoSnO_3$ in degrading methylene blue dye was assessed under sunshine and UV-light exposure using varying weight percentages of the catalyst. The rGO/ $CoSnO_3$ nanocomposite exhibits superior degrading efficiency (96.2%) in comparison to bare materials such as Co_3O_4 (83.6%) and $CoSnO_3$ (85.8%). Sunlight is a more favorable source for eco-friendly photocatalytic degradation processes when compared to UV-light and sunlight irradiation. According to electrochemical studies, $CoSnO_3$ and rGO/ $CoSnO_3$ electrodes have notable areal capacitance values of 158.8 F/g and 499.7 F/g at a scan rate of 10 mV/s, respectively. The rGO/ $CoSnO_3$ electrode exhibited a higher specific capacitance of 603.12 F/g at 1 A/g compared to the $CoSnO_3$ electrode, which had a specific capacitance of 285.3 F/g at 1 A/g, as indicated by their charge-discharge curves. The rGO/ $CoSnO_3$ electrode demonstrates a 95.7% cycle retention rate, even after 1000 cycles. The symmetrical electrode device demonstrated that rGO/ $CoSnO_3$ has higher capacitance compared to pure $CoSnO_3$. Calculating the manufactured nano materials for usage as a capacitor in energy storage and for minimizing water pollution through efficient photodegradation processes.

5. References

1. Xudong L, Shufan C, Zhengwei X, Kailin L, Yuxin Z. Tungsten oxide-based nanomaterials for supercapacitors: Mechanism, fabrication, characterization, multifunctionality and electrochemical performance. Progress in Material Science; c2022.
2. Kang M, Zho H. Facile synthesis and structural characterization of Co_3O_4 nanocubes. Aims Materials Science; c2015. p. 16-27.
3. Shi-jie Lu, Zhi-teng W, Xia-hui Z, Zhen-jiang H, Hui T, Yun-jiao Li, *et al*. In Situ-Formed Hollow Cobalt Sulfide Wrapped by Reduced Graphene Oxide as an Anode for High-Performance Lithium-Ion Batteries. American Chemical Society Applied Materials & Interfaces; c2019.
4. Yanjie W, Juliana A, Torres S, Meital C, Marcelo H, Tao Caue. Photocatalytic materials applications for sustainable agriculture. Progress in Material Science; c2022.
5. Vennela AB, Mangalaraj D, Muthukumarasamy N, Agilan A, Hemalatha KV. Structural and optical properties of Co_3O_4 nanoparticles prepared by sol-gel technique for photocatalytic application. International Journal of Electrochemical Science; c2019. p. 3535-3552.
6. Posudievsky OY, Khazieieva O, Koshechko V, Pokhodenko D. Preparation of graphene oxide by solvent-free mechanochemical oxidation of graphite. Journal of Materials Chemistry; c2012.
7. Sharifi S, Shakur HR, Mirzaei A, Salmani A, Hosseini MH. Characterization of cobalt oxide Co_3O_4 nanoparticles prepared by various methods: Effect of calcination temperatures on size, dimension, and catalytic decomposition of hydrogen peroxide. International Journal of Nanoscience and Nanotechnology; c2013. p. 51-58.
8. Vangari M, Pryor T, Jiang L. Supercapacitors: Review of Materials. Journal of Energy Engineering (C); c2013. p. 72-79.
9. Liu Q, Yang H, Zhi-hua Liu, Gang L. Preparation of SnO_2- Co_3O_4 biochar catalyst as a lewis acid for corncob hydrolysis into furfural in water medium. Journal of Industrial and Engineering Chemistry; c2015. p. 49-54.
10. Rui Li, Chang Z, Mengqiao X. Novel hierarchical structural SnS_2 composite supported by biochar carbonized from chewed sugarcane as enhanced anodes for lithium-ion batteries. Journal of Springer Nature; c2020. p. 1239-1247.
11. Suganya P, Princy J, Mathivanan N, Krishnasamy K. One-Pot Synthesis of rGO@Cu2V2O7 Nanocomposite as High Stabled Electrode for Symmetric Electrochemical Capacitors. ECS Journal of Solid State Science and Technology; c2022. p. 041005.
12. Subhalaxmi M, Shantikumar V, Nair V, Kumar R. Synthesis of Co_3O_4 Nanoparticles Wrapped Within Full Carbon Matrix as an Anode Material for Lithium-Ion Batteries. Acta Metallurgica Sinica (English Letters); c2017.
13. Guanghui A, Yue A, Jiandi Liu A, Han J, Qin D, Chen Q, *et al*. Amorphous $CoSnO_3$@rGO nanocomposite as an efficient cathode catalyst for long-life batteries. Chinese Journal of Catalysis. 2018;39:1951-1959.
14. Hao H, Shi J, Jang S, Reza-Ugalde A, Hani Naguib E. Hierarchically Structured Nitrogen-Doped Multilayer Reduced Graphene Oxide for Flexible Intercalated Supercapacitor Electrodes. American Chemical Society Energy Materials; c2020. p. 987-997.
15. Saba A, Jamil, Hasnaat Ahmad A, Shafiq-ur-Rehman A, Shanza Rauf Khan A, Janjua MRSA. The first morphologically controlled synthesis of a nanocomposite of graphene oxide with cobalt tin oxide nanoparticles. RSC Advances; c2018.
16. Yuanling M, Yulong M, Wang. Plasma-Assisted Simultaneous Reduction and Nitrogen/Sulfur Codoping of Graphene Oxide for High-Performance Supercapacitors. ACS Sustainable Chemistry & Engineering; c2019. p. 7597-7608.
17. Manikandan V, Elancheran R, Revathi P, Vanitha U, Suganya P, Krishnasamy K. Synthesis, characterization, photocatalytic and electrochemical studies of reduced graphene oxide-doped nickel oxide nanocomposites. Asian Journal of Chemistry. 2021;33:411-422.
18. Mani V, Periasamy AP, Chen MS. Highly selective amperometric nitrite sensor based on chemically reduced graphene oxide modified electrode. Electrochemistry Communications; c2012. p. 75-78.
19. Narayanan DP, Gopalakrishnan A, Yaakob Z, Sugunan S, Narayanan BN. A Facile Synthesis of Clay-Graphene Oxide Nanocomposite Catalysts for Solvent-Free Multicomponent Biginelli Reaction. Arabian Journal of Chemistry; c2017.
20. Adetayo A, Runsewe D. Synthesis and Fabrication of Graphene and Graphene Oxide: A Review. Open Journal of Composite Materials; c2019. p. 207-229.
21. Dideikin AT, Vul AY. Graphene Oxide and Derivatives: The Place in Graphene Family. Frontiers in Physics; c2019, 149.
22. Mohamed Barakat Z, Dehua Z, Ulf-peter A, Takahiro N,

Refaie E, Kenawy N, *et al*. Dual-Heteroatom-Doped Reduced Graphene Oxide Sheets Conjoined Co-Ni-Based Carbide and Sulfide Nanoparticles for Efficient Oxygen Evolution Reaction. American Chemical Society; c2020. p. 40186-40193.
23. Tian J, Wu J, Yin X, Wu W. Novel preparation of hydrophilic graphene/graphene oxide nanosheets for supercapacitor electrode. Applied Surface Science; c2019. p. 496,-143696.
24. Zhai Y, Wei W, Hu H, Jing J, Lv X, Xu W, *et al*. Reduced graphene oxide decorated $CoSnO_3$@$ZnSnO_3$ with multi-component double-layered hollow nanoboxes for high energy storage and capacity retention asymmetric supercapacitors. Journal of Alloys and Compounds; c2020.
25. Khan MS, Yadav R, Vyas R. Synthesis and evaluation of reduced graphene oxide for supercapacitor application. Materials Today: Proceedings; c2020.
26. Chubei W, Jianwei Z, Feipeng. Synthesis of Highly Reduced Graphene Oxide for Supercapacitor. Journal of Nanomaterials; c2016.
27. Posudievsky Oleg Yu, Oleksandra Khazieieva A, Yacheslav V, Koshechko K, Vitaly Pokhodenko D. Preparation of graphene oxide by solvent-free mechanochemical oxidation of graphite. Journal of Materials Chemistry; c2012. p. 12465-12467.
28. Suganya P, Princy J, Mathivanan N and Krishnasamy K. Hydrothermal Synthesis of Nickel Vanadate Nanorod for Outstanding Energy Storage Application. Indian Journal of Natural Sciences, 2022, 13-40363.
29. Zhou D, Cheng P, Luo J, Xu Z, Li L, Yuan D. Facile synthesis of graphene@NiMoO4 nanosheet arrays on Ni foam for a high-performance asymmetric supercapacitor. Journal of Materials Science. 2017;52:13909-13919.
30. Lee YT, Lee E, Lee JM, Lee W. Micro-sized pH sensors based on patterned Pd structures using an electrolysis method. Current Applied Physics; c2009. p. 218-221.
31. Ahmed Ali AM, Ahmed NM, Mohammad SM, Sabah FA, Kabaa E, Alsadig A, *et al*. Effect of gamma irradiation dose on the structure and pH sensitivity of ITO thin films in extended gate field effect transistor. Results in Physics; c2019. p. 615-622.